JCI The Journal of Clinical Investigation

Lipotoxicity disrupts incretin-regulated human β cell connectivity

David J. Hodson, … , Stephen J. Hughes, Guy A. Rutter

J Clin Invest. 2013;123(10):4182-4194. https://doi.org/10.1172/JCI68459.

Research Article **Endocrinology**

Pancreatic β cell dysfunction is pathognomonic of type 2 diabetes mellitus (T2DM) and is driven by environmental and genetic factors. β cell responses to glucose and to incretins such as glucagon-like peptide-1 (GLP-1) and glucose-dependent insulinotropic polypeptide (GIP) are altered in the disease state. While rodent β cells act as a coordinated syncytium to drive insulin release, this property is unexplored in human islets. In situ imaging approaches were therefore used to monitor in real time the islet dynamics underlying hormone release. We found that GLP-1 and GIP recruit a highly coordinated subnetwork of β cells that are targeted by lipotoxicity to suppress insulin secretion. Donor BMI was negatively correlated with subpopulation responses to GLP-1, suggesting that this action of incretin contributes to functional β cell mass in vivo. Conversely, exposure of mice to a high-fat diet unveiled a role for incretin in maintaining coordinated islet activity, supporting the existence of species-specific strategies to maintain normoglycemia. These findings demonstrate that β cell connectedness is an inherent property of human islets that is likely to influence incretin-potentiated insulin secretion and may be perturbed by diabetogenic insults to disrupt glucose homeostasis in humans.

Lipotoxicity disrupts incretin-regulated human β cell connectivity

David J. Hodson,[1] Ryan K. Mitchell,[1] Elisa A. Bellomo,[1] Gao Sun,[1] Laurent Vinet,[2] Paolo Meda,[2] Daliang Li,[3] Wen-Hong Li,[3] Marco Bugliani,[4] Piero Marchetti,[4] Domenico Bosco,[5] Lorenzo Piemonti,[6] Paul Johnson,[7] Stephen J. Hughes,[7] and Guy A. Rutter[1]

[1]Section of Cell Biology, Division of Diabetes, Endocrinology and Metabolism, Department of Medicine, Imperial College London, London, United Kingdom.
[2]Department of Cell Physiology and Metabolism, University of Geneva School of Medicine, Geneva, Switzerland.
[3]UT Southwestern Medical Center, Dallas, Texas, USA. [4]Department of Endocrinology and Metabolism, University of Pisa, Pisa, Italy.
[5]Cell Isolation and Transplantation Center, Department of Surgery, Geneva University Hospitals and University of Geneva, Geneva, Switzerland.
[6]Diabetes Research Institute (HSR-DRI), San Raffaele Scientific Institute, Milan, Italy.
[7]Nuffield Department of Surgical Sciences, University of Oxford, Oxford, United Kingdom.

Pancreatic β cell dysfunction is pathognomonic of type 2 diabetes mellitus (T2DM) and is driven by environmental and genetic factors. β cell responses to glucose and to incretins such as glucagon-like peptide-1 (GLP-1) and glucose-dependent insulinotropic polypeptide (GIP) are altered in the disease state. While rodent β cells act as a coordinated syncytium to drive insulin release, this property is unexplored in human islets. In situ imaging approaches were therefore used to monitor in real time the islet dynamics underlying hormone release. We found that GLP-1 and GIP recruit a highly coordinated subnetwork of β cells that are targeted by lipotoxicity to suppress insulin secretion. Donor BMI was negatively correlated with subpopulation responses to GLP-1, suggesting that this action of incretin contributes to functional β cell mass in vivo. Conversely, exposure of mice to a high-fat diet unveiled a role for incretin in maintaining coordinated islet activity, supporting the existence of species-specific strategies to maintain normoglycemia. These findings demonstrate that β cell connectedness is an inherent property of human islets that is likely to influence incretin-potentiated insulin secretion and may be perturbed by diabetogenic insults to disrupt glucose homeostasis in humans.

Introduction

Type 2 diabetes mellitus (T2DM) currently affects approximately 8.3% of the adult population worldwide, an incidence expected to increase further in the coming years (1). Changes in functional pancreatic β cell mass, the sole source of circulating insulin in vertebrates, are characteristic of this condition and act in concert with defective insulin action to reduce glucose tolerance in genetically susceptible individuals (2). Increased circulating levels of glucose, fatty acids, and other reactive species then drive the complications of this disease including stroke, cardiovascular disease, retinopathy, renal failure, and cancer (3, 4).

The mechanisms underlying glucose-stimulated insulin secretion (GSIS) from single β cells are increasingly well characterized and involve uptake of the sugar via specific glucose transporters (5), enhanced ATP synthesis (6), and the closure of ATP-sensitive K^+ channels (K_{ATP}) (7). The consequent plasma membrane depolarization leads to Ca^{2+} influx (8) and exocytosis from secretory granules (9), further potentiated by "K_{ATP}-independent" signals (10). In addition to glucose, a range of other secretagogues, including gut-derived incretins, serve to amplify insulin release. Thus, in response to food transit, glucagon-like peptide-1 (GLP-1) and glucose-dependent insulinotropic polypeptide (GIP) (11) are released by enteroendocrine L and K cells, respectively, from where they augment GSIS to counteract the postprandial hyperglycemic spike (12–15). This so-called "incretin effect" requires elevated glycemia, and GLP-1 and GIP receptor activation engages intracellular signaling mechanisms largely dependent on cyclic adenosine monophosphate (cAMP) generation (16–18) and activated Ca^{2+} influx (19). Since incretins also stimulate antiapoptotic and prosurvival pathways in β cells (20), GLP-1 mimetics and dipeptidyl peptidase-4 (DPP-4) inhibitors have become first-line antihyperglycemic agents for the treatment of T2DM (21). However, both GLP-1– and GIP-induced insulin secretion are impaired in T2DM (22–25), and patients may respond nonoptimally to both endogenous and exogenous incretin.

Efforts to better understand the interactions that drive GLP-1–augmented (and GIP-augmented) insulin secretion from intact islets have, however, proved challenging due to a lack of uniformity in microorgan architecture between species. This is evident in both the proportions and spatial organization of β, α, and other cell types (26). Phylogenetic differences in insulin secretion may consequently arise from heterogeneity in the intraislet regulation of β cell dynamics, alongside the simple summation of distinct cell biophysical properties. Thus, in humans, the release of insulin from ensembles of stochastically-behaving β cells is likely to reflect their unique cytoarchitectural arrangement along laminar epithelial sheets, combined with alterations to paracrine and neural input (27–30). As such, rodents may represent a nonideal model for investigations of human pancreatic β cell dysfunction, especially if diabetogenic insults perturb species-specific intraislet mechanisms governing β cell population responses.

Using in situ imaging approaches, together with large-scale correlation analyses to map cell-cell interconnectivity (31), we demonstrate that GLP-1 recruits a highly coordinated subnetwork of β cells to augment GSIS, and this is targeted by lipotoxic insults to reduce insulin secretion. Providing evidence for an association with circulating lipid levels in humans, donor BMI was found to be negatively correlated with the coordinated β cell

Conflict of interest: The authors have declared that no conflict of interest exists.
Citation for this article: *J Clin Invest.* 2013;123(10):4182–4194. doi:10.1172/JCI68459.

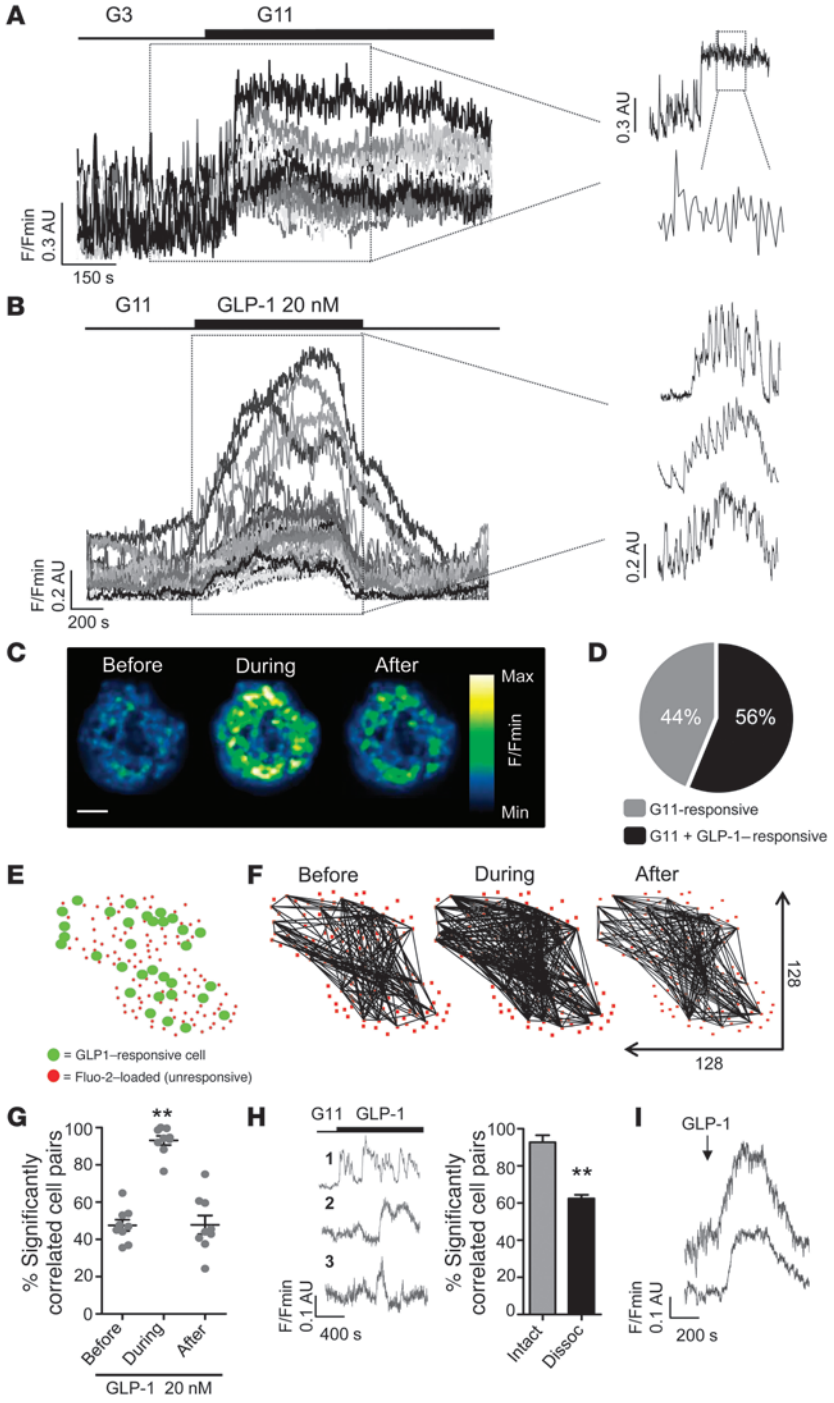

Figure 1

GLP-1 activates a highly coordinated subnetwork of β cells. (**A**) β cells display largely stochastic Ca^{2+} oscillations following elevation of glucose concentrations (G11; 11 mM glucose). (**B**) Functional multicellular Ca^{2+} imaging (fMCI) reveals highly coordinated β cell responses to stimulation with 20 nM GLP-1 (G11, 11 mM glucose). (**C**) A pseudocolored human islet before, during, and after application of GLP-1 in the presence of permissive glucose concentrations (11 mM glucose; recording time = 40–60 minutes; image cropped to display a single islet). Scale bar: 50 μm. (**D**) Pie chart displaying the proportion of glucose-responsive β cells (identified following transition from 3 to 11 mM glucose) that further responded to GLP-1 with Ca^{2+} rises of at least 20% above the baseline (n = 4 recordings). (**E**) Cartesian map depicting x-y coordinates of GLP-1–responsive cells (green) within intact islets (red dots = fluo-2–loaded, but GLP-1–unresponsive cells). (**F**) As for **E**, but weighted graph depicting location and number of significantly correlated cell pairs before, during, and after GLP-1 application (Pearson R, $P < 0.05$; scale, pixels). (**G**) Mean percentage of significantly correlated cell pairs transiently increases during the application of GLP-1 (**$P < 0.01$ versus before; Kruskal-Wallis test, n = 9 islets from 4 donors). (**H**) Dissociation (Dissoc) of islets impairs correlated responses to GLP-1 (1, 2, 3 = cell 1, cell 2, and cell 3, respectively; **$P < 0.01$ versus intact; Mann-Whitney U test; n = 8 slides from 3 donors). (**I**) As for **H**, but representative traces from a cell pair that remained connected following dissociation. F/Fmin, normalized fluorescence.

responses to GLP-1. We believe, therefore, that these results reveal a novel mode of incretin action that may be targeted by known T2DM risk factors to impact insulin release from human islets.

Results

GLP-1 activates a coordinated subpopulation of β cells. Multicellular calcium (Ca^{2+}) imaging was used to simultaneously monitor Ca^{2+} signals emanating from fluo-2–loaded β cells residing within the first few layers of intact human islets (Supplemental Figure 1A [supplemental material available online with this article; doi:10.1172/JCI68459DS1]; for data from n = 21 separate normoglycemic donors, see Supplemental Table 1; donors across the BMI range were selected for experiments using multiple preparations). Since exocytosis in electrically excitable endocrine cells is Ca^{2+} dependent (32), the effects of intervention on the cell population dynamics underlying insulin release were determined by subjecting the resulting traces to large-scale correlation analyses (31). We note that, although α and other neuroendocrine cells comprise a substantial proportion (~40%) of the human islet (26), the former are unlikely to contribute to the recordings here, since elevated glucose is expected to have no effect or to reduce intracellular free Ca^{2+} concentrations ($[Ca^{2+}]_i$) in these cells (33).

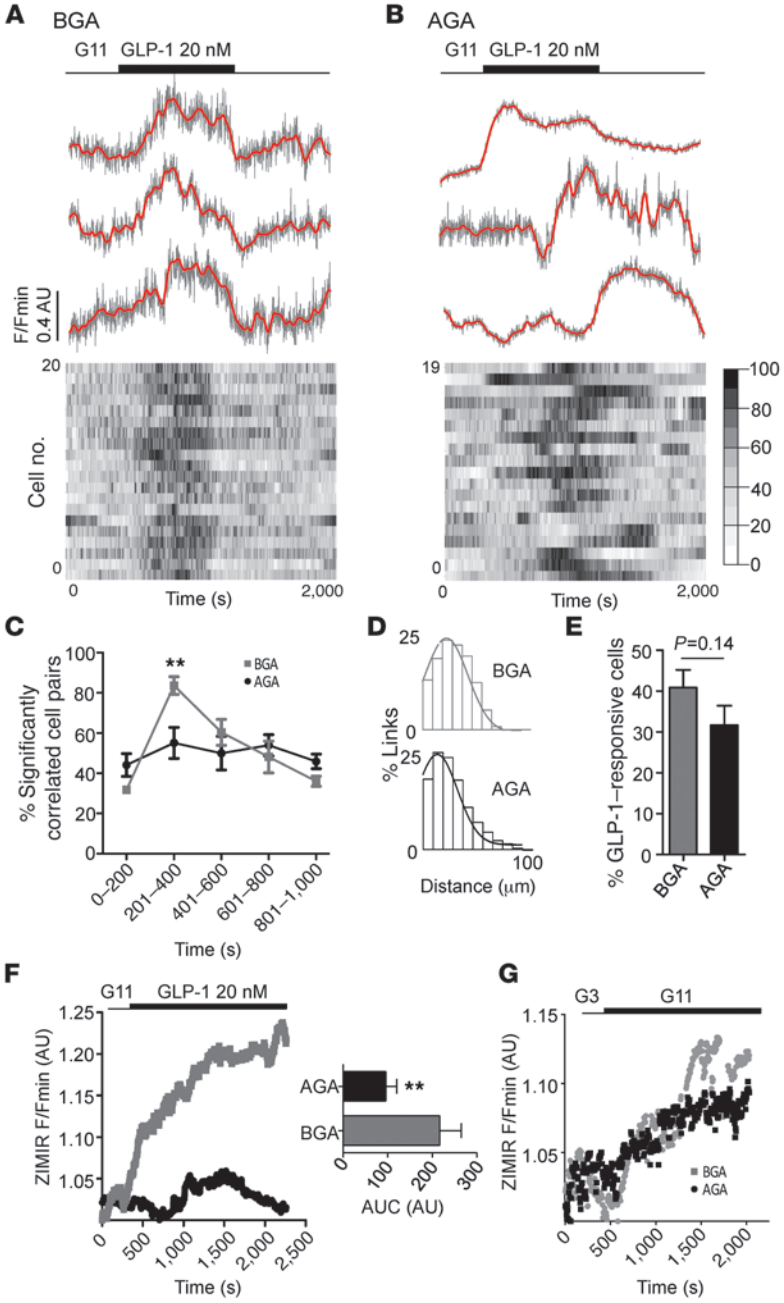

Figure 2

Gap junctions coordinate cell responses to GLP-1. (**A**) BGA, an inactive analog of the GJ blocker AGA, does not affect coordinated β cell responses to 11 mM glucose (G11) plus GLP-1. Top panel: representative Ca^{2+} traces; red, smoothed; gray, raw. Bottom panel: heatmap depicting minimum (0) to maximum (100) for each cell. (**B**) As for **A**, except the application of AGA induces asynchrony in the GLP-1–treated population, which presents as lagged responses to stimulus. (**C**) Histogram showing the mean percentage of significantly correlated cell pairs in BGA- and AGA-treated islets before (0–200 seconds), during (201–400 seconds), and after (401–1,000 seconds) GLP-1 application (**$P < 0.01$ versus AGA; two-way ANOVA; $n = 8$ islets from 3 donors). (**D**) Probability histograms of distances between correlated β cell pairs in BGA-treated (top panel) and AGA-treated (bottom panel) islets. AGA decreases the distances over which cells coordinate their activity as demonstrated by the left-shifted Gaussian peak (curve fitted to binned data from 3 donors). (**E**) AGA does not significantly alter the mean percentage of GLP-responsive cells ($P = 0.14$; Mann-Whitney *U* test). (**F**) AGA decreases GLP-1–stimulated insulin release measured in real time using the Zn^{2+}-sensitive probe ZIMIR (left panel; mean traces from 3 donors). Bar graph (right panel) showing decreased mean AUC in AGA-treated islets (**$P < 0.01$; Mann-Whitney *U* test; $n = 7–8$ islets from 3 donors). (**G**) 11 mM glucose-stimulated (G11-stimulated) insulin secretion is identical in AGA- and BGA-treated islets (representative traces from $n = 4$ recordings).

Long-lasting optical recordings (30–60 minutes) revealed that, in the presence of elevated (11 mM) glucose, β cells displayed moderate levels of coordinated activity due to stochastic Ca^{2+} oscillations, as previously reported (Figure 1A and refs. 27, 34). Following the application of 10 fM–100 nM (peak response 20 nM) GLP-1 (7-36 human amide; Supplemental Figure 1, B–E), large and synchronous deflections in $[Ca^{2+}]_i$ were associated with dramatic improvements in coordinated β-β cell activity (Figure 1B and C; Supplemental Video 1). This was due to the recruitment of a subpopulation of GLP-1–responsive cells (~56% of glucose-responsive cells, assumed to be β cells, Figure 1D and E) whose levels of correlated Ca^{2+}-spiking activity could be dynamically and transiently modified by incretin in a glucose-dependent and GLP-1 receptor–dependent (GLP-1R–dependent) manner (43.6 ± 2.7 versus 92.8 ± 3.7% significantly correlated cell pairs, before and during GLP-1 20 nM application, respectively; $n = 9$ islets from 4 donors, $P < 0.01$; Figure 1F and G; Supplemental Figure 2). The 3D tissue context was essential for supporting GLP-1–driven upregulation of coordinated cell activity, since this was reduced to almost control levels (~60%) in dissociated islets (Figure 1H). The residual synchronization likely reflects both the presence of cells (10%–20%) that remained physically connected (Figure 1I) and the random probability of synchronous activity in otherwise unconnected cells.

Gap junctions orchestrate spatiotemporally precise responses to GLP-1. Next, we attempted to define the intercellular mechanisms underlying the orchestrated propagation of GLP-1–derived Ca^{2+}

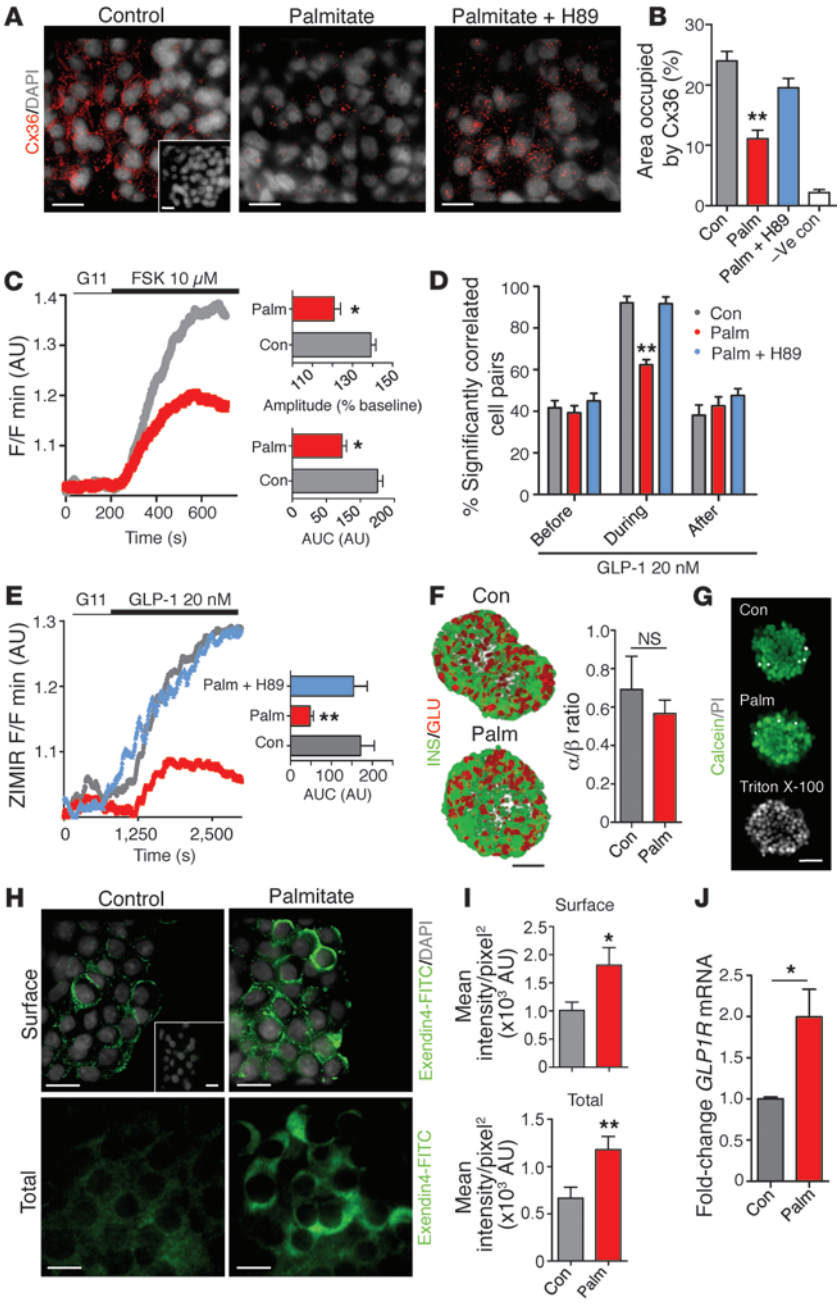

Figure 3

Lipotoxicity disrupts cell-cell communication to impair GLP-1 responses. (**A**) 72-hour exposure to palmitate reduces Cx36 expression, and this can be reversed by coincubation with the PKA inhibitor H89 (negative control, inset). Scale bars: 10 μm (including inset). (**B**) Fraction area occupied by Cx36 is reduced in palmitate-treated (Palm) islets in a PKA-dependent manner (Palm + H89) (**P < 0.01 versus control [Con], Kruskal-Wallis test; n = 19 islets from 3 donors). (**C**) Palmitate blunts cell responses to forskolin (FSK). Left panel: mean traces; right panel: AUC and amplitude. (*P < 0.05 versus control; Mann-Whitney U test; n = 6 recordings). (**D**) Lipotoxicity decreases coordinated cell responses to GLP-1 in a PKA-dependent manner (**P < 0.01, 2-way ANOVA; n = 8 islets from 3 donors). (**E**) GLP-1–stimulated insulin secretion is impaired following palmitate exposure. Left panel: representative traces; right panel: AUC (**P < 0.01, Kruskal-Wallis test; n = 8–12 islets from 3 donors). (**F**) Left panel: 3D opacity projection of islets immunolabeled for insulin (INS) and glucagon (GLU). Right panel: FFA does not alter the α/β ratio (NS versus control; Mann-Whitney U test; n = 4 islets from 2 donors). Scale bar: 75 μm. (**G**) Dead/live ratio is unaffected by palmitate (n = 17 islets). Scale bar: 50 μm. (**H**) FFA exposure increases surface (top) and total (bottom) GLP-1R number (n = 7–18 islets from 3 donors). Scale bars: 15 μm (including inset). (**I**) Mean intensity values of surface (top) and total (bottom) exendin-4 FITC are significantly increased by incubation with palmitate (*P < 0.05, **P < 0.01 versus control; Mann-Whitney U test). (**J**) Similarly, FFA increases *GLP1R* mRNA expression (*P < 0.05 versus control; Mann-Whitney U test).

signaling events between β cells. Homotypic gap junctions (GJs) composed of connexin 36 (Cx36) are present between human and rodent β cells (35, 36) and play an important role in coordinating the cell-cell information exchanges that underlie pulsatile insulin release from rodent islets (36, 37). Application of the GJ blocker, 18-α-glycyrrhetinic acid (AGA), but not its inactive analog β-glycyrrhizic acid (BGA), induced asynchrony in the incretin-sensitive subpopulation (Figure 2, A and B) and significantly reduced the ability of β cells to mount coordinated Ca^{2+} rises in the presence of GLP-1 (83.6 ± 4.4 versus 55.10 ± 7.7% significantly correlated cell pairs at 200 seconds, BGA versus AGA, respectively; n = 8 islets from 3 donors, P < 0.01; Figure 2C). The GJ blocker appeared to be relatively specific, since preincubation of islets with AGA: (a) reduced the distance between correlated cell pairs from 30 μm to 20 μm, consistent with an effect on GJ-coupling conduction and impedance (38) (Gaussian curve fitted to histogram of n = 3 donors; Figure 2D); (b) did not affect the percentage of GLP-1–responsive cells (Figure 2E); (c) was unable to significantly alter intracellular Ca^{2+} rises in response to 11 mM glucose or 20 mM KCl (Supplemental Figure 3, A and B, respectively); and (d) yielded identical results to experiments in which gene expression was silenced in β cells by greater than 80% using shRNA against human Cx36 (Supplemental Figure 4). GJ blockade severely diminished incretin-stimulated (Figure 2F), but not glucose-stimulated, insulin secretion (117.3 ± 12.7 versus 132.7 ± 18.6 AU, BGA versus AGA, respectively; n = 4 recordings, NS) (Figure 2G) measured

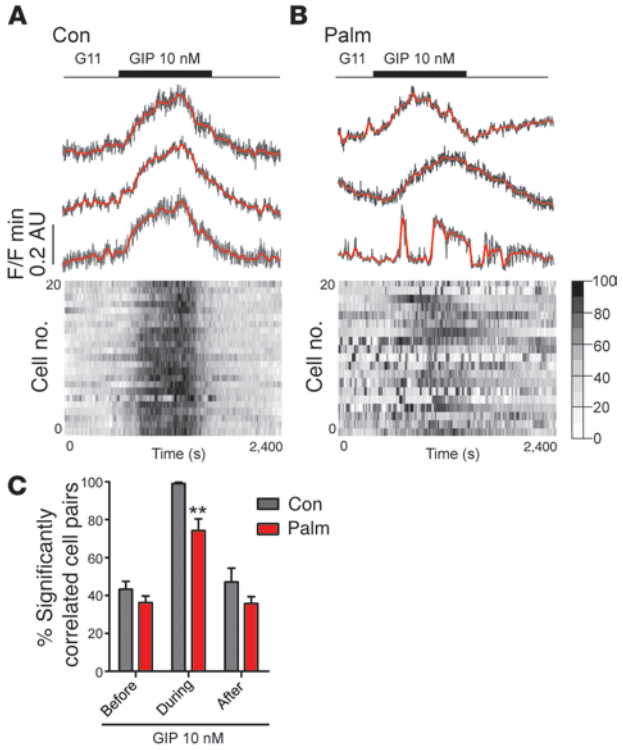

Figure 4
Palmitate disrupts coordinated responses to GIP. (**A**) β cell responses to stimulation with 10 nM GIP are highly coordinated under control conditions (G11, 11 mM glucose). Top panel: representative Ca^{2+} traces; red, smoothed; gray, raw. Bottom panel: heatmap depicting minimum (0) to maximum (100) for each cell. (**B**) As for **A**, except following 72-hour exposure to palmitate. Note the asynchronous responses in the GIP-responsive population. (**C**) Lipotoxic conditions significantly disrupt coordinated cell responses to GIP (**$P < 0.01$, two-way ANOVA; n = 11–12 islets from 3 donors).

using the sensitive membrane-tethered zinc (Zn^{2+}) probe ZIMIR (39), suggesting that GLP-1 may drive insulin release by improving correlated activity within a subpopulation of β cells (Supplemental Videos 2 and 3).

Lipotoxicity targets the incretin-sensitive β cell subpopulation to impair insulin secretion. To assess whether this novel mode of incretin action might be targeted by diabetogenic insults, we incubated human islets under lipotoxic conditions (40–42), namely in the presence of high levels of the free fatty acid (FFA) palmitate. The effectiveness of the saturated fatty acid was confirmed by the upregulation of mitochondrial uncoupling protein 2 *(UCP2)* mRNA expression (1.00 ± 0.04 versus 1.95 ± 0.24 relative mRNA expression, control versus palmitate, respectively; n = 3 donors; $P < 0.05$) (43). As previously observed for rodent islets (44), 72-hour incubation with palmitate markedly reduced Cx36 protein expression in a protein kinase A–dependent (PKA-dependent) manner (24.0 ± 1.6 versus 11.1 ± 1.4% area occupied by Cx36, control versus palmitate, respectively; $P < 0.01$ (Figure 3, A and B, and Supplemental Figure 5). In parallel, acute Ca^{2+} responses to forskolin, an adenyl cyclase (AC) activator that improves electrotonic coupling between β cells through the generation of cAMP (45), were attenuated by exposure to FFAs (Figure 3C; n = 6 recordings). In addition to blunting GSIS (Supplemental Figure 6; n = 5 recordings) and consistent with its effects on Cx36 expression, palmitate reduced the coordinated activity in response to GLP-1 in a PKA-dependent manner (Figure 3D and Supplemental Figure 7), decreasing the portion of insulin secretion attributable to incretin (i.e., above and beyond that stimulated by 11 glucose alone; AUC = 171.4 ± 33.4 versus 48.0 ± 8.0 AU, control versus palmitate, respectively; n = 8–12 islets from 3 donors, $P < 0.01$; Figure 3E). Although GLP-1 actions are in part mediated by PKA, confounding effects of residual blockade were unlikely, given that the islets were washed for at least 1 hour before imaging, incretin-stimulated insulin secretion (ISIS) was normal in H89-treated human samples, and acute application of the inhibitor failed to alter GLP-1–induced Ca^{2+} rises (Supplemental Figure 8).

The deleterious effects of lipotoxicity were unlikely to be secondary to signal transmission through an altered or necrotic islet core, since islet architecture and cell viability both remained constant, as indicated by the α/β cell (Figure 3F) and dead/live cell ratios (0.025 ± 0.006 versus 0.020 ± 0.005, control versus palmitate, respectively, NS; n = 17 islets from 2 to 3 donors) (Figure 3G). Moreover, the observed effects of FFAs were highly reproducible between individual islet preparations (Supplemental Figure 9) and were not due to a reduction in GLP-1 receptor (GLP-1R) expression. Thus, cell surface and total GLP-1R levels (n = 7–18 islets from 3 donors; $P < 0.05$) (Figure 3H and I; Supplemental Figure 10), and receptor transcript expression (1.00 ± 0.02 versus 2.00 ± 0.33 relative mRNA expression, control versus palmitate, respectively; n = 7 replicates from 3 donors; $P < 0.01$) (Figure 3J) both increased in response to FFAs. We found that palmitate also impaired the correlated responses to GIP (Figure 4), suggesting that incretin-regulated β cell connectivity represents a conserved process that is vulnerable to lipotoxicity. Last, we confirmed the dynamic secretion measures obtained using ZIMIR by radioimmunoassay-based (RIA-based) measures of insulin release during static incubation of islets (Figure 5).

Excess FFAs do not disrupt global islet responses to other β cell stimuli. Given that various stimuli have been shown to alter the coordinated activity of rodent β cells (46, 47), we determined whether lipotoxicity might perturb human islet dynamics to reduce insulin release evoked by glucose or a range of nonfuel secretagogues. FFAs appeared to specifically target incretin action primarily through the disruption of β cell interactivity, since impairment of insulin

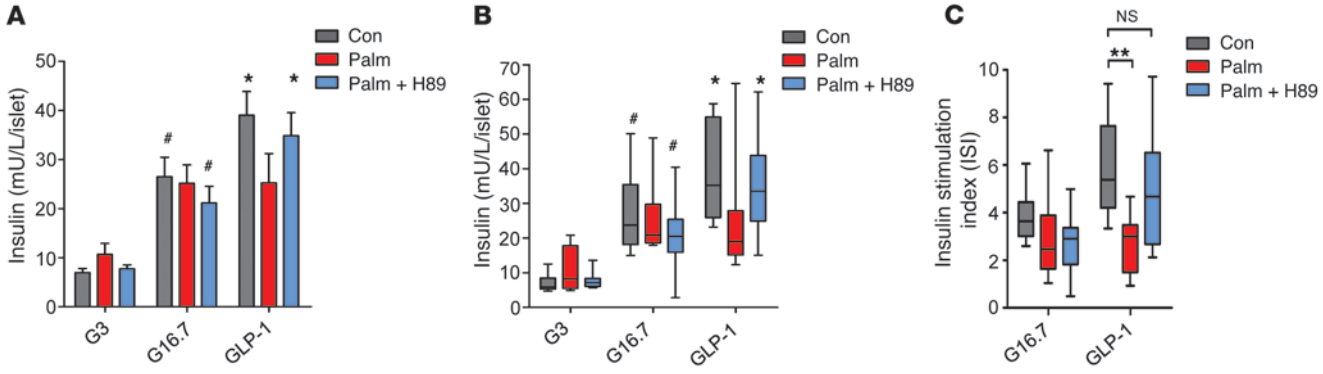

Figure 5

FFAs suppress GLP-1–stimulated insulin secretion. (**A**) GLP-1 potentiates insulin secretion in control islets, and this is abolished by palmitate in a PKA-dependent manner (Palm + H89) (#P < 0.01 versus 3 mM glucose [G3] and *P < 0.05 versus 16.7 mM glucose [G16.7]; one-way ANOVA). Values represent the mean ± SEM. (**B**) As for **A**, but box-and-whisker plot (box = first and third quartiles; whisker = range) showing data distribution around the median. (**C**) As for **B**, but with ISI to better account for the variation between islet preparations from different isolation centers (**P < 0.01 and NS versus palmitate; two-way ANOVA). Data are from 6 independent experiments using islets from 4 donors.

secretion by palmitate (Supplemental Figure 6) was not accompanied by decreases in the percentage of active cells (Figure 6A), frequency of Ca^{2+} oscillations (Figure 6, B and C), amplitude and AUC of $[Ca^{2+}]_i$ rises (Figure 6D), or long-term evolutions in coordinated activity (Figure 6E; correlation calculated over 20 to 30 minutes) in response to elevated (11 mM) glucose (n ≥4 islets from 3 donors). Likewise, we observed that lipotoxicity did not affect changes in cytosolic free Ca^{2+} detected in response to the non-metabolic depolarizing stimulus tolbutamide (Figure 6F) or the inositol 1,4,5-*tris*phosphate-generating (IP_3-generating) muscarinic agonist carbachol (Figure 6H). The coordinated $[Ca^{2+}]_i$ rises elicited by both drugs were not disrupted by FFA exposure (Figure 6G and I; n = 4 recordings) or GJ blockade (Supplemental Figure 11), suggesting that they were likely due to simultaneous depolarization throughout the recorded β cell population.

Incretin-induced upregulation of coordinated cell activity is species specific. To determine whether the above findings in human islets might be recapitulated in a physiological model of in vivo FFA excess, we examined the effects of diet-induced obesity (DIO) in mice. As expected, islets isolated from C57/BL6 mice fed a high-fat diet (HFD) (60% calories from fat) for at least 18 weeks to elevate circulating FFA concentrations presented severe glucose intolerance (Supplemental Figure 12A) and mild downregulation of Cx36 (Supplemental Figure 12B), as previously shown (48), without affecting cell viability (Supplemental Figure 12C; n = 5–10 animals) (49). Over half (53%) of the islets from the HFD animals displayed disorganized Ca^{2+} oscillations in response to high (11 mM) glucose (Supplemental Videos 4 and 5), yet retained apparently normal control GLP-1 responses that resembled those from human islets (Figure 7A). Further analyses of these HFD-responsive islets yielded a significant decrease in the coordination of glucose-induced Ca^{2+} oscillations compared with those from animals fed a normal diet (ND) (90.8 ± 2.9 versus 58.0 ± 5.2% significantly correlated cell pairs before GLP-1 application, ND versus HFD, respectively; n = 8 islets from 4 animals, P < 0.01) (Figure 7B). This deficit was reversed by the application of GLP-1, as evidenced by restoration of normal levels of coordinated cell activity (Figure 7B) and subtly improved ISIS (355.5 ± 27.2 versus 487.4 ± 30.2 AU, ND versus HFD, respectively; n = 12 islets from 4 animals, P < 0.01) (Figure 7C). Calculation of the duty cycle revealed that ISIS in the ND animals was associated with increased time spent in the active phase, rather than any changes in correlated cell-cell Ca^{2+}-spiking activity (Figure 7D). These observations could be mimicked by the exogenous application of palmitate to isolated mouse islets (Figure 7, E–G, and Supplemental Figure 13), confirming a direct action of the lipid on the rodent β cell to impair coordinated responses to glucose. Therefore, the exaggerated FFA levels associated with an HFD are unlikely to primarily target ISIS. Instead, the oral glucose intolerance detected in these mice may result from impaired GSIS and/or defective insulin action rather than a diminished incretin effect (49).

BMI is negatively associated with coordinated responses to GLP-1. To investigate whether the FFA-impaired incretin responses detected in vitro were present in human islets exposed in vivo to excess circulating lipid, as observed with increasing obesity (50), we examined the relationship between the BMI of individual organ donors and GLP-1–stimulated β cell activity. We detected a significantly negative linear correlation between donor BMI (spanning the normal-obese range) and coordinated β cell responses to GLP-1 (Figure 8A; R^2 = –0.88, P < 0.001). In contrast, the age of the same individuals did not correlate with GLP-1–coordinated β cell responses (Figure 8B; R^2 = –0.07, P = 0.37).

Discussion

The principal aim of the current study was to determine whether β cell-β cell coordination is an important element in the response of human islets to secretagogues. We show that efficient ISIS from intact human islets relies on driving high levels of coordinated activity in a 3D organized subnetwork of GJ-interlinked β cells. This hitherto unknown mode of incretin action is targeted in vitro by lipotoxicity, an insult strongly associated with T2DM risk and one that has previously been shown to result in defective GSIS (40, 41). Specifically, chronic exposure to elevated FFAs reduces insulin release by disrupting intercellular communications, impeding the timely propagation of signals throughout the GLP-1–sensitive syncytium (see Supplemental Figure 14 for a schematic illustration). Donor BMI was negatively associated with coordinated islet responses to GLP-1, suggesting that this novel

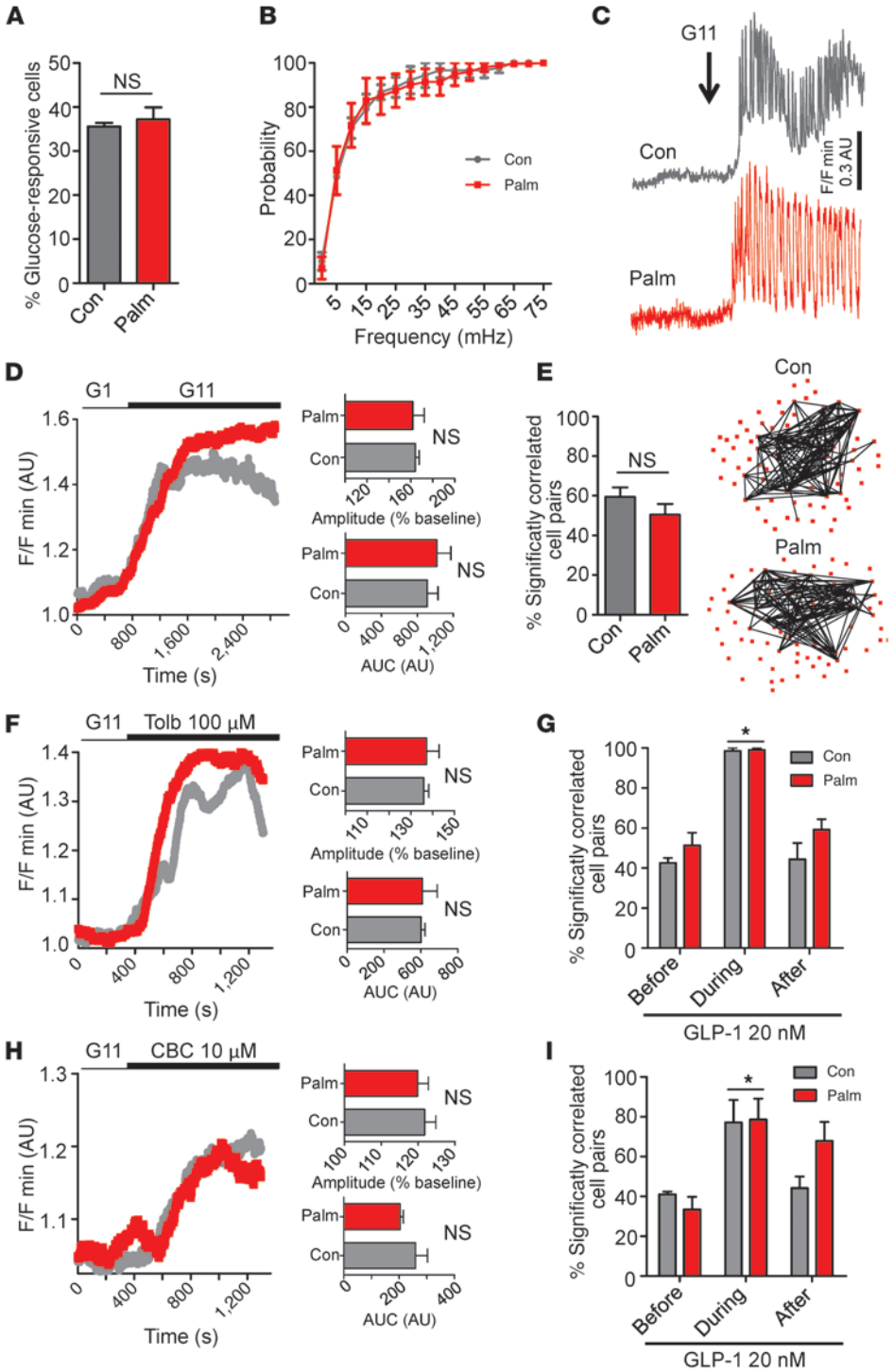

Figure 6
Global islet responses to glucose and other stimuli are unaffected by FFA exposure. (**A**) Exposure to palmitate does not alter the percentage of glucose-responsive cells versus control (NS versus control; Mann-Whitney *U* test; $n = 4$ islets from 3 donors). (**B**) Cumulative probability histogram demonstrates identical distribution of Ca^{2+} oscillation frequencies in control- and palmitate-treated islets (NS; two-way ANOVA; $n = 4$ islets from 3 donors). (**C**) Representative Ca^{2+} traces from glucose-responsive cells. (**D**) Palmitate treatment does not alter the kinetics of glucose-induced cytosolic Ca^{2+} rises (left panel: mean traces), as shown by graphs of amplitude and AUC (right panels) (NS versus control; Mann-Whitney *U* test; $n = 4$ islets from 3 donors). (**E**) The extent (left panel) and distribution (right panel) of correlated activity in response to elevated glucose is unchanged by FFA exposure (NS versus control; Mann-Whitney *U* test; $n = 4$ islets from 3 donors). (**F**) Palmitate does not affect Ca^{2+} responses to tolbutamide (Tolb) (left panel: mean traces), as shown by graphs of the amplitude and AUC (NS versus control; Mann-Whitney *U* test; $n = 4$ recordings). (**G**) Palmitate-exposed islets display normal correlated responses following the application of tolbutamide (*$P < 0.05$ versus before GLP-1 for each treatment; Kruskal-Wallis test; $n = 4$ recordings). (**H**) As for **F**, but in the presence of carbachol (CBC) (NS versus control; Mann-Whitney *U* test; $n = 3$–4 islets from 3 donors). (**I**) As for **G**, but following the application of carbachol (*$P < 0.05$ versus before GLP-1 for each treatment; Kruskal-Wallis test; $n = 3$–4 islets from 3 donors).

mode of incretin action may also be perturbed by excess circulating lipids in humans.

An increasing body of work indicates that β cell responses to GLP-1 are altered during T2DM in both lean and obese individuals (22–24, 51), changes further compounded by the inheritance of T2DM risk alleles (52). Direct evidence that lipotoxicity represents a primary step in reducing the sensitivity of pancreatic β cells to GLP-1 in human subjects has, however, been difficult to obtain, given the effects of lipotoxicity to raise circulating glucose levels and to decrease GLP-1 secretion from the gut (53). Our results, based on both in vitro and in vivo analyses, strongly suggest that lipotoxicity may impair β cell responses to both GLP-1 and GIP independently of glucotoxicity. The current findings also corroborate recent in vivo studies in which the incretin effect was found to be attenuated in obese individuals with normal glucose tolerance and GLP-1 output (25). Thus, diminished incretin sensitivity

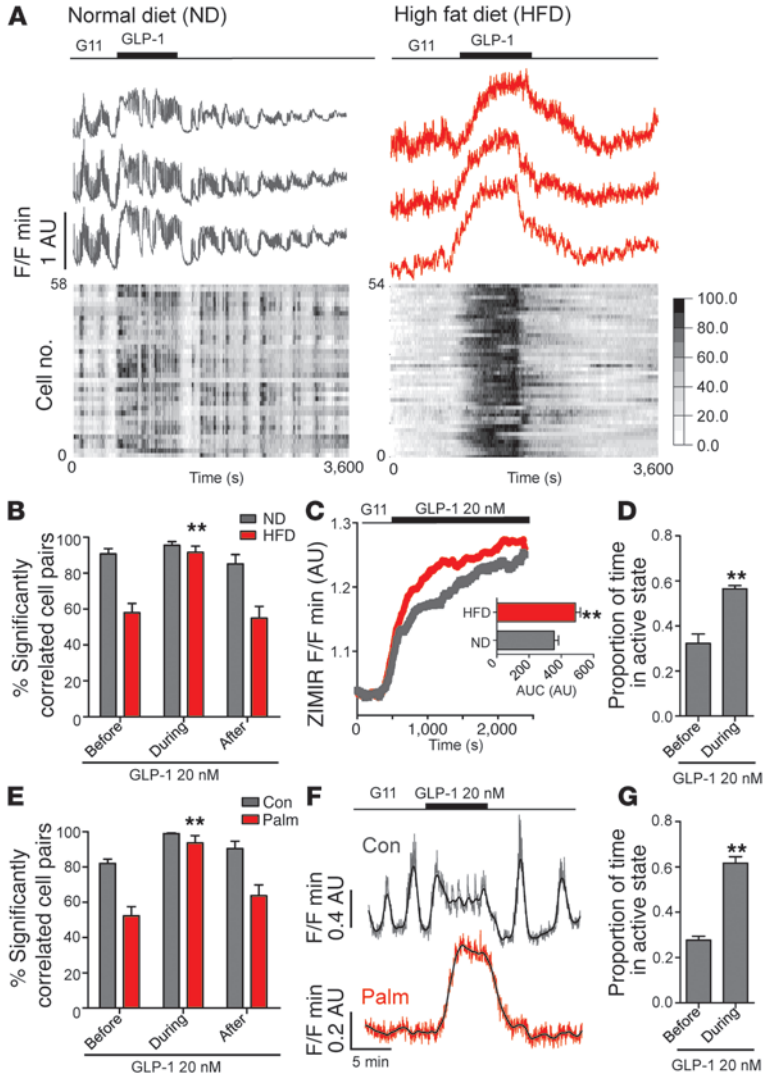

Figure 7

Species specificity of incretin action on coordinated β cell activity. (**A**) β cells within islets from ND animals display highly coordinated Ca^{2+} oscillations in response to 11 mM glucose (G11), and synchronicity is not affected by 20 nM GLP-1. Conversely, an HFD disrupts G11-stimulated coordinated β cell activity, but this is restored by the application of incretin. Top panel: representative Ca^{2+} traces. Bottom panel: heatmap depicting minimum (0) to maximum (100) for each cell. (**B**) Bar graph demonstrating that the mean percentage of significantly correlated cell pairs is restored to ND values during the application of GLP-1 to islets derived from HFD-fed animals (**$P < 0.01$ versus before GLP-1 application, Kruskal-Wallis test; $n = 8$ islets from at least 4 animals). (**C**) GLP-1–stimulated insulin secretion (G11; 11 mM glucose), as measured using ZIMIR, is subtly improved by an HFD (**$P < 0.01$ versus ND, Mann-Whitney U test; $n = 12$ islets from 4 animals). (**D**) Duty cycle (i.e., time spent in the active phase) is 2-fold higher during the application of GLP-1 to islets from ND animals (**$P < 0.01$ versus before GLP-1 application; Mann-Whitney U test; $n = 4$ recordings). (**E**) As for **B**, except for the exogenous application of palmitate to islets from animals fed an ND (**$P < 0.01$ versus before GLP-1 application; Kruskal-Wallis test; $n = 8$ islets from 6 animals). (**F**) Representative traces from control- and palmitate-treated islets. (**G**) As for **D**, except for the exogenous application of control (BSA plus NaOH) to islets from animals fed an ND (**$P < 0.01$ versus before GLP-1 application; Mann-Whitney U test).

is likely to represent an early event in T2DM pathogenesis in obese individuals, contributing to, rather than being a consequence of, more widespread β cell dysfunction.

The deleterious effects of FFAs on the islet dynamics underlying insulin release appear to be manifested through PKA- and cAMP-dependent inhibition of cell-cell GJ coupling. While our data suggest that lipotoxicity provokes a seemingly paradoxical reduction in cAMP and an elevation in PKA, this should be considered in light of the complexities inherent in this G_s subunit–operated signaling cascade (54). For example, palmitate may increase PKA activity through an AC isoform distinct from those upregulated by forskolin, chronic FFA-induced increases in cAMP/PKA may not reflect the suppression of maximal forskolin-mediated AC stimulation, and lipids can activate PKA via cAMP-independent pathways including those mediated by sphingosine accumulation (55–57). Nevertheless, given that GLP-1 and GIP engage cAMP, a messenger shown to acutely improve electrical transfers between β cells (45), and given that Ca^{2+} responses to forskolin were blunted by palmitate exposure in our experiments, it is reasonable to hypothesize that FFAs may target the islet dynamics underlying ISIS with two interrelated modes of action: impairment of GJ communications via a chronic effect of PKA on Cx36 protein expression (44), and inhibition of the augmented electrotonic coupling observed in response to fleeting challenge with cAMP-elevating ligands such as GLP-1 (45). Further functional dissection of the exact mechanisms involved will require the use of cAMP-monitoring recombinant probes that can be adapted for cell-specific expression throughout intact human islets (58).

Demonstrating a predilection for the cell-cell interactions involved in incretin action, FFA treatment did not similarly influence responses to glucose or other stimuli. Whereas tolbutamide and carbachol coordinated cell activity, presumably through mass depolarization of the islet syncytium, their actions were unaffected by either palmitate or GJ blockade. This observation suggests that the heterogeneity of GLP-1R expression, the second messenger characteristics, and the degree of connexin impairment all contribute to the GJ dependency of the incretin. The finding that FFAs reduce GSIS may therefore stem from summation at the single-cell level of the dissociation of membrane-proximate Ca^{2+} hotspots from exocytosis (59, 60), rather than any effects on global $[Ca^{2+}]_i$ and/or islet synchrony.

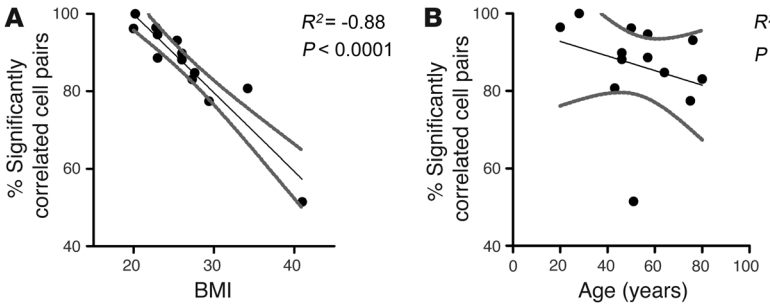

Figure 8
BMI is negatively correlated with coordinated responses to 20 nM GLP-1. (**A**) BMI of individual donors (n = 13; i.e., those used for control Ca^{2+} recordings) was plotted as a function of the mean coordinated cell activity in response to GLP-1 application (R^2 = 0.88, P < 0.001; linear regression). (**B**) As for **A**, but age (R^2 = 0.07, P = 0.37; linear regression). Gray lines, 95% CI.

Although we used chiefly lipotoxic conditions throughout the present study, it remains to be determined whether "glucolipotoxic" conditions (i.e., elevated glucose and fatty acids) (40, 41) exert similar or more severe effects on connectivity. In any case, the mechanisms by which (gluco)lipotoxicity impacts the genes involved in β cell-β cell communication such as *Cx36* are still largely obscure, but may involve enhanced peroxisomal fatty acid oxidation, production of ROS, and repression of cAMP-response elements (44, 61).

We asked whether the incretin-regulated changes in β cell cooperativity we observed in human islets might also be present in rodent systems, and thus ultimately be amenable to more straightforward physiological and genetic dissection. β cells within mouse islets are arranged into "small-world" networks and, in response to glucose, display explosive increases in cytosolic Ca^{2+} levels that rhythmically spread throughout the population as autoregenerative oscillatory wavefronts (62–64). Since these activity dynamics underlie insulin secretion, as inferred from animal models presenting with disorganized cell activity (36, 37, 46), attention has been focused on elucidating the mechanisms underlying the intraislet regulation of β cell function in the rodent setting. However, β cells residing within human islets behave in a more stochastic manner, with coordination present only in small cell ensembles and no apparent large-scale synchrony when viewed at the population level (27, 34). Although human islets possess differing paracrine and neural regulation of intercellular communication (29, 30), similarities to their murine counterparts nonetheless exist, such as β cell–specific expression of Cx36 and the extent of β cell dye coupling (35). The current finding that incretin responses in intact human islets display marked GJ dependency therefore raises the intriguing possibility that insulin secretion from human islets is more reliant on an enhancement of coordinated β cell activity by non-sugar secretagogues. Indeed, mice consume small, frequent meals, particularly after lights out, whereas food intake in humans is strongly entrained to the light phase, when it occurs as 3 to 4 meals (65). Thus, an evolutionarily advantageous link between blood glucose levels and food intake may be imprinted on human islets in the form of phylogenetic differences in the mechanisms that regulate incretin responsiveness.

Of note was the observation that obese mice possessed glucose and incretin responses similar to those seen in human islets, since the maintenance of mice on an HFD perturbed coordinated responses to glucose that could be rescued by GLP-1 application. Lipids mildly reduced Cx36 expression in these animals, so the restorative effect of GLP-1 on cell-cell communications may stem from either continued transmission through the remaining GJs, or upregulation of GJ-independent signaling mechanisms (see ref. 66 for a discussion of possible mechanisms). Consequently, rather than representing a paradigm of exposure to excess FFAs, hypertrophied islets from HFD-fed animals may instead more closely model the default human scenario, albeit with subtle differences in the structural and functional regulation of ISIS (26). These species-specific differences may reflect diet-adapted strategies to maintain normoglycemia in the face of nutrient oversupply, since the proportion of energy intake attributable to fat is almost two-fold lower in mice than in humans (~13% [1] versus 25% [7] fat [saturated fat]).

Conversely to our findings in human islets, palmitate has been shown to subtly downregulate receptor mRNA expression in isolated mouse islets (67), although this did not appear to alter the fold change in ISIS. Of interest, an endogenous GLP-1 system has recently been reported in human islets, and tissue isolated from T2DM donors displayed upregulated incretin release (68). Consistent with the latter finding, increased GLP-1R expression may therefore represent a compensatory mechanism to maintain ISIS in the face of compromised GSIS in humans. While these data further underscore the species divergence in incretin signaling, overinterpretation should be avoided in the absence of GLP-1R quantification by Western blotting, an approach currently precluded by the lack of specific antibodies against either mouse or human receptor epitopes (69).

In summary, these results characterize a new aspect of human islet behavior involved in the normal responsiveness to secretagogues and a likely contributor to insulin secretory failure in T2DM. Since reduced GLP-1–stimulated insulin secretion is a feature of T2DM associated with both obesity and risk alleles (22, 25, 52), changes in incretin-regulated β cell cooperativity, which we describe here, may provide a unifying mechanism through which multiple factors such as lifestyle and genes can impact insulin release to reduce β cell function in humans.

Methods

Animal studies. Animals were maintained in a pathogen-free facility under a 12-hour light/12-hour dark cycle with free access to water and food. For the HFD treatment, 8-week-old C57/BL6 mice were placed on chow containing 60% wt/wt fat content (Lillico Biotechnology). At 15 weeks of feeding, the animals were starved overnight before being subjected to an intraperitoneal glucose tolerance test (IPGTT) (1g/kg D-glucose) to confirm the efficacy of the HFD in promoting glucose intolerance.

Cell culture. Human islets obtained from normoglycemic donors at isolation centers in Oxford, Geneva, Milan, and Pisa were cultured in RPMI supplemented with 5.5 mM D-glucose, 10% FCS, 100 U penicillin, 100 μg streptomycin, and 0.25 μg/μl fungizone (37°C, 5% CO_2). Islets were treated for 72 hours with either control (BSA plus NaOH), 0.5 mM BSA-conju-

gated palmitate or 0.5 mM BSA-conjugated palmitate plus 10 μM H89 (PKA inhibitor; Tocris). For the GJ inhibition studies, islets were preincubated for 1 hour with AGA or its inactive analog BGA (both 20 μM; Sigma-Aldrich) before imaging. Studies have shown this dose to effectively disrupt GJ signaling in intact islets (70). Mice were euthanized by cervical dislocation, and pancreatic islets were isolated by collagenase digestion (71). Islets were cultured for 24 to 48 hours as above, but in RPMI supplemented with 11 mM instead of 5.5 mM glucose, and containing no fungizone.

Calcium imaging. Isolated islets were incubated (37°C, 95% O_2/5% CO_2) for 30 minutes in fluo-2-AM (10 μM) diluted with a mixture of DMSO (0.01%, wt/vol) and pluronic acid (0.001%, wt/vol; all from Invitrogen) in a bicarbonate buffer solution (120 mM NaCl, 4.8 mM KCl, 1.25 mM NaH_2PO_4, 24 mM $NaHCO_3$, 2.5 mM $CaCl_2$, 1.2 mM $MgCl_2$, and 3 mM D-glucose). Following acclimatization to the indicated glucose concentration, islets were placed on glass coverslips in a custom-manufactured aluminum chamber (Digital Pixel) mounted on a Zeiss Axiovert coupled to a Nipkow spinning-disk head (Yokogawa CSU-10) and equipped with objectives adjusted for chromatic aberration (10×–20×/0.3–0.5 NA, EC Plan-Neofluar; Zeiss). Whole-islet multicellular Ca^{2+} imaging was performed as previously described (31). Briefly, Ca^{2+} dynamics were captured with cellular resolution from the 50–200 fluo-2–loaded cells residing within the first and second layers of the intact islets. Use of a spinning disk to rapidly scan large areas of the islet allowed events to be recorded for long periods with minimal phototoxicity. A solid-state laser (CrystaLaser) controlled by a laser-merge module (Spectral Applied Physics) provided wavelengths of 491 nm to excite fluo-2 (rate = 0.5Hz; exposure time = 263 ms). Emitted light was filtered at 525/50 nm, and images were captured by a highly sensitive 16-bit, 512 × 512 pixel back-illuminated EM-CCD camera (ImageEM 9100-13; Hamamatsu). Volocity software (PerkinElmer) provided the user interface. During recording, islets were maintained at 35°C to 36°C and continuously irrigated with bicarbonate buffer aerated with 95% O_2/5% CO_2. GLP-1 (7-36 human amide fragment), tolbutamide, forskolin, carbachol, AGA, BGA (all from Sigma-Aldrich), GIP (human), and exendin 9-39 (both from Bachem) were delivered via the perfusion system at the doses indicated in the figures and accompanying legends.

Real-time imaging of insulin release. Insulin release was monitored using ZIMIR as previously described (39). Briefly, before imaging, islets were incubated for 2 hours in ZIMIR (1 mM), a membrane-bound probe that fluoresces upon binding of zinc (Zn^{2+}) coreleased with insulin from granules. During recording, islets were irrigated with bicarbonate buffer containing 1 μM EGTA to improve the signal-to-noise ratio (SNR) without affecting intracellular Ca^{2+} or Zn^{2+} concentrations (39). Excitation was delivered at 491 nm (rate = 0.2 Hz; exposure = 1 second), and emitted signals were collected at 525/50 nm. Islets were arbitrarily subdivided into 10 to 20 regions, and the normalized (F/F_{min}) intensity over time was calculated for each region. Islet-wide insulin release dynamics were then represented by the mean intensity over time and the AUC, calculated by ignoring peaks less than 20% of the distance from minimum-to-maximum *y* to account for fluctuations in the baseline due to the SNR.

Insulin secretion assays. Six human islets were incubated in duplicate for 30 minutes in 1 ml of Krebs-HEPES-bicarbonate (KHB) solution (130 mM NaCl, 3.6 mM KCl, 1.5 mM $CaCl_2$, 0.5 mM $MgSO_4$, 0.5 mM NaH_2PO_4, 2 mM $NaHCO_3$, 10 mM HEPES, and 0.1 % [wt/vol] BSA, pH 7.4) at 37°C containing the indicated glucose and GLP-1 concentrations. A specific RIA for human insulin (Millipore) was used to measure hormone released into the medium.

Immunohistochemistry. Islets were fixed overnight at 4°C in PFA (4%, wt/vol) before the application of primary antibodies (1:1,000 mouse antiglucagon or 1:200 guinea pig anti-insulin; both from DAKO). Following overnight incubation at 4°C, islets were washed, incubated for 2 hours at room temperature with a secondary antibody (goat anti-rabbit Alexa 488 or goat anti-guinea pig Alexa 568, both 1:500; Invitrogen), and mounted on Superfrost slides (Fisher Scientific) using Vectashield DAPI-containing mounting medium (Vector Labs). For Cx36 staining, an identical protocol was used, except that islets were fixed and permeabilized for 3 minutes using acetone before incubation with primary (rabbit anti-Cx36, 1:50) and secondary (donkey anti-rabbit Alexa 488, 1:500) antibodies (both from Invitrogen).

Fluorophores were excited using a high-magnification objective (63×/1.4 NA, Plan-Apochromat DIC; Zeiss) and 491-nm and 561-nm laser lines in single-track mode. DAPI was visualized at 359 nm using the epifluorescent port of the microscope. In all cases, emitted signals were detected using filters centered on 480/40 nm, 535/30 nm, and 630/75 nm for DAPI, Alexa 488, and Alexa 568, respectively. The α/β cell ratio was determined by subjecting the resulting images to automated thresholding (threshold plugin for ImageJ software) and dividing the α cell area by the β cell area. Similarly, the fraction area occupied by Cx36 was calculated by dividing the threshold-corrected Cx36 immunopositive area by the total image area. Uniform linear adjustments were applied to contrast and brightness to improve image quality for analysis and presentation purposes, while preserving the pixel dynamic range and the intersample intensity differences.

Synthesis and validation of exendin-4 FITC. An exendin-4 FITC (on K12) peptide was custom synthesized according to the following sequence: HGEGTFTSDLSK(*FITC*)QMEEEAVRLFIEWLKNGGPSSGAPPPS (GenicBio Limited). C57/BL6 mice were injected i.v. with 8 nmol/200 μl of the peptide, sacrificed 1 hour after injection with a lethal dose of pentobarbital, and immediately perfused via the left ventricle with 4% PFA. The pancreas was then cryosectioned and immunolabeled for insulin (guinea pig anti-insulin Igs, 1:200; Ventrex), glucagon (mouse anti-glucagon Igs, 1:2,000; Sigma-Aldrich), and FITC to enhance the exendin signal (rabbit anti-FITC Igs, 1:100; Invitrogen). The secondary antibodies used were anti-guinea pig Igs coupled to Dylight 405 (1:800; Jackson ImmunoResearch Laboratories), anti-mouse Igs coupled to TRITC (1:500; SouthernBiotech), and anti-rabbit Igs coupled to Alexa 488 (1:500; Invitrogen) for insulin, glucagon, and exendin, respectively. To estimate the GLP-1R number at the cell surface in human islets, 100 nM exendin-4 FITC diluted in PBS was applied for 1 hour at 4°C (to minimize internalization) before rinsing and processing for immunohistochemistry. To assess total GLP-1R binding, islets were permeabilized with 1.5 mM Triton X-100 before application of exendin-4 FITC. Specificity was verified by preincubating islets for 10 minutes with excess 1 μM GLP-1.

Lentiviral delivery of shRNA. Commercially validated lentiviral particles carrying shRNA expression constructs against human *GJD2* were acquired from Sigma-Aldrich (NM_020660; clone IDs: TRCN000074089, TRCN000074092, TRCN0000413941, and TRCN000436198). MOI was calculated using Turbo-GFP particles (Sigma-Aldrich). Specificity of *GJD2* gene silencing was confirmed using quantitative PCR (qPCR). In all cases, nontargeting lentiviral particles containing scrambled shRNA were used as negative controls (Sigma-Aldrich).

Real-time PCR. Total RNA was extracted in TRIzol reagent and reverse transcribed using a high-capacity cDNA reverse transcription kit (both from Invitrogen). The relative mRNA abundance was quantified by qPCR using SYBR Green Master Mix and a 7500 fast real-time PCR engine (both from Invitrogen). Primers (Supplemental Table 2) were designed not to span genomic DNA sequences using PerlPrimer. Specificity was validated using a dissociation curve, and linear amplification of both target and housekeeping genes was tested using a dilution series. The expression of each gene was normalized to cylcophilin A (*Ppia*), and relative changes in mRNA expression versus control were calculated using the comparative Ct method ($2^{-[delta][delta]}$Ct).

Western immunoblotting. Islets were washed in ice-cold PBS before lysis in precipitation assay buffer (50 mM Tris HCl, pH 8.0, 150 mM NaCl, 1% nonidet P-40, 0.5% sodium deoxycholate, 0.1% SDS) and sonication. Total protein extracts were resolved using a 12% SDS-PAGE gel (12% Tris-acrylamide), wet transferred onto a PVDF membrane, and subjected to immunoblotting using either rabbit anti-Cx36 (1:50; Invitrogen) or mouse monoclonal antitubulin (1:5,000; Sigma-Aldrich clone B-5-1-2). Revelation was performed using HRP-linked anti-rabbit antibodies (1:10,000; GE Healthcare) and a proprietary ECL detection reagent.

Live/dead assay. Islets were incubated for 15 minutes in PBS containing 3 μM calcein AM (Invitrogen) and 2.5 μM propidium iodide (PI) (Sigma-Aldrich) before detection of absorbance/emission at 491/525 nm and 561/620 nm, respectively. The islet area occupied by dead cells (PI) was calculated and expressed as a unitary ratio versus that occupied by live cells (calcein).

Correlation analysis. Correlation analyses were performed using a Pearson *R* coefficient as previously detailed (72). Briefly, individual fluo-2–loaded cells were identified using a region of interest (ROI), and intensity over time traces and Cartesian (*x-y*) coordinates were extracted. The resulting datasets were imported into R (R project, R Development Core Team) and IgorPro (Wavemetrics), baseline trends were removed by fitting a linear equation, and intensity values were normalized. GLP-1–responsive cells were manually filtered on the basis of a sustained rise in $[Ca^{2+}]_i$ levels above a 10% threshold to account for SNR. Subsequent to this, the one-sided correlation function between all possible cell pair combinations (excluding the autocorrelation) was assessed using the Pearson's product moment correlation defined by Equation 1, where *x* and *y* represent cells 1 and 2, respectively.

$$r = \frac{\sum xy}{\sqrt{\sum x^2 \sum y^2}} \quad \text{(Equation 1)}$$

Significance ($P < 0.05$) was determined against the expected *t* distribution of independent *R* values (with two degrees of freedom). The location of significantly correlated cell pairs was displayed on a weighted graph constructed using the Cartesian (*x-y*) coordinates of each cell. Phase maps were compiled by converting the normalized intensity (minimum = 0; maximum = 100) of each cell to a color corresponding to a user-generated light-dark 256-color ramp.

Frequency and duty cycle analysis. Ca^{2+}-spiking frequency was measured as previously described (31). Briefly, power spectrums based on the fast Fourier transform (FFT) were constructed for each cell, a confidence interval of 95% was imposed, and the frequency with the highest significant power was extracted. A histogram of frequency (mHz) was then plotted for each state. To assess the proportion of time spent in the "ON" phase, traces from each experiment were binarized using a 10% threshold and duty cycle (*D*), calculated using Equation 2, where τ and T represent the time spent in the active phase and total time, respectively. The mean *D* values were then compared between the different treatment states.

$$D = \frac{\tau}{T} \quad \text{(Equation 2)}$$

Statistics. In all cases, data distribution was determined using a D'Agostino omnibus test. Non-Gaussian data were analyzed using either a Mann-Whitney *U* test or, where multiple comparisons were required, a Kruskal-Wallis test (followed by a Dunn's post-hoc test). Normally distributed data were analyzed using a two-tailed Student's *t* test or one-way ANOVA followed by a Bonferroni's post-hoc test (accounting for degrees of the freedom). Between-treatment effects were assessed using two-way ANOVA followed by a Bonferroni's post-hoc test. Linear correlations were calculated using regression analyses. Analysis was performed using R, GraphPad Prism (GraphPad Software), IgorPro, and MATLAB (MathWorks). $P < 0.05$ was considered statistically significant, and values represent the mean ± SEM unless otherwise stated.

Study approval. All studies involving human tissue were approved by the National Research Ethics Committee (NRES) London (Fulham) "Signal transduction in isolated human islets: regulation by glucose and other stimuli" (REC 07/H0711/114). Islets were isolated under the approval of NRES Oxfordshire (REC 09/H0605/2) (Oxford, United Kingdom), Comitato di Bioetica Azienda Ospedaliero-Universitaria Pisana (34058) (Pisa, Italy), Comitato Etico Istituto Scientifico San Raffaele (Milan, Italy), and the Central Institutional Review Board on Clinical Research of Geneva University Hospitals (CER 05-028 [05-065]) (Geneva, Switzerland). Where required, consent from next of kin was obtained before use of tissue for scientific research. Animal procedures were approved by the Home Office according to the Animals (Scientific Procedures) Act 1986 of the United Kingdom (PPL 70/7349) and/or the Geneva Veterinary Office (Geneva, Switzerland; authorization 1034/3552/1).

Acknowledgments

Studies were supported by a Diabetes UK R.D. Lawrence Research Fellowship (12/0004431; to D.J. Hodson); a Wellcome Trust Senior Investigator grant (WT098424AIA); the MRC Programme (MR/J0003042/1); a Diabetes UK Project Grant (11/0004210); and Royal Society Wolfson Research Merit Awards (to G.A. Rutter); the Swiss National Science Foundation (310030_141162; and CR32I3_129987); Juvenile Diabetes Research Foundation (JRDF) (5-2012-281; 99-2012-775) and EU FP7 (BETAIMAGE 222980; BETATRAIN 289932) awards (to P. Meda); and JDRF (37-2011-21) and NIH (R01-GM077593) awards (to W-H. Li). The work leading to this publication has received support from the Innovative Medicines Initiative Joint Undertaking under grant agreement 155005 (IMIDIA), resources of which are composed of financial contributions from the European Union's Seventh Framework Programme (FP7/2007-2013) and EFPIA companies' in kind contribution (to G.A. Rutter and P. Meda). Isolation of human islets was supported by JDRF awards (31-2008-416, to D. Bosco and 31-2008-413 to L. Piemonti) (European Consortium for Islet Transplantation, ECIT). We are also grateful to Francesca Semplici, Timothy Pullen, and Gabriela Da Silva Xavier for their useful advice on molecular biology. Last, we thank Patrice Mollard, Pierre Fontanaud, and Francois Molino of the Institut de Genomique Fonctionnelle, Montpellier, France, for their assistance with analysis.

Received for publication December 21, 2012, and accepted in revised form July 11, 2013.

Address correspondence to: David J. Hodson, Section Cell Biology, Department of Medicine, Imperial College London, London SW7 2AZ, United Kingdom. Phone: 44.0.20.7594.1713; Fax: 44.0.20.7594.3351; E-mail: d.hodson@imperial.ac.uk. Or to: Guy A. Rutter, Section of Cell Biology, Department of Medicine, Imperial College London, London SW7 2AZ, United Kingdom. Phone: 44.0.20.7594.3340; Fax: 44.0.20.7594.3351; E-mail: g.rutter@imperial.ac.uk.

1. International Diabetes Federation. *IDF Diabetes Atlas*. 5th ed. Brussels, Belgium: International Diabetes Federation; 2011.
2. Prentki M, Nolan CJ. Islet beta cell failure in type 2 diabetes. *J Clin Invest*. 2006;116(7):1802–1812.
3. Currie CJ, Poole CD, Gale EA. The influence of glucose-lowering therapies on cancer risk in type 2 diabetes. *Diabetologia*. 2009;52(9):1766–1777.
4. Stitt AW. AGEs and diabetic retinopathy. *Invest Ophthalmol Vis Sci*. 2010;51(10):4867–4874.
5. McCulloch LJ, van de Bunt M, Braun M, Frayn KN, Clark A, Gloyn AL. GLUT2 (SLC2A2) is not the principal glucose transporter in human pancreatic beta cells: implications for understanding genetic association signals at this locus. *Mol Geneti Metab*. 2011; 104(4):648–653.
6. Tarasov AI, et al. The mitochondrial Ca2+ uniporter MCU is essential for glucose-induced ATP increases in pancreatic beta-cells. *PLoS One*. 2012; 7(7):e39722.
7. Hattersley AT, Ashcroft FM. Activating mutations in Kir6.2 and neonatal diabetes: new clinical syndromes, new scientific insights, and new therapy. *Diabetes*. 2005;54(9):2503–2513.
8. Grapengiesser E, Gylfe E, Hellman B. Dual effect of glucose on cytoplasmic Ca2+ in single pancreatic beta-cells. *Biochem Biophys Res Commun*. 1988; 150(1):419–425.
9. Tsuboi T, Rutter GA. Multiple forms of "kiss-and-run" exocytosis revealed by evanescent wave microscopy. *Curr Biol*. 2003;13(7):563–567.
10. Henquin JC. The dual control of insulin secretion by glucose involves triggering and amplifying pathways in beta-cells. *Diabetes Res Clin Pract*. 2011; 93(suppl 1):S27–S31.
11. Phillips LK, Prins JB. Update on incretin hormones. *Ann N Y Acad Sci*. 2011;1243:E55–E74.
12. Holst JJ. The physiology of glucagon-like peptide 1. *Physiol Rev*. 2007;87(4):1409–1439.
13. Baggio LL, Drucker DJ. Biology of incretins: GLP-1 and GIP. *Gastroenterology*. 2007;132(6):2131–2157.
14. Seino Y, Fukushima M, Yabe D. GIP and GLP-1, the two incretin hormones: Similarities and differences. *J Diabetes Invest*. 2010;1(2):8–23.
15. Lamont BJ, Li Y, Kwan E, Brown TJ, Gaisano H, Drucker DJ. Pancreatic GLP-1 receptor activation is sufficient for incretin control of glucose metabolism in mice. *J Clin Invest*. 2012;122(1):388–402.
16. MacDonald PE, El-Kholy W, Riedel MJ, Salapatek AM, Light PE, Wheeler MB. The multiple actions of GLP-1 on the process of glucose-stimulated insulin secretion. *Diabetes*. 2002;51(suppl 3):S434–S442.
17. Hansotia T, et al. Double incretin receptor knockout (DIRKO) mice reveal an essential role for the enteroinsular axis in transducing the glucoregulatory actions of DPP-IV inhibitors. *Diabetes*. 2004; 53(5):1326–1335.
18. Furman B, Ong WK, Pyne NJ. Cyclic AMP signaling in pancreatic islets. *Adv Exp Med Biol*. 2010; 654:281–304.
19. Leech CA, et al. Molecular physiology of glucagon-like peptide-1 insulin secretagogue action in pancreatic beta cells. *Prog Biophys Mol Biol*. 2011; 107(2):236–247.
20. Li Y, Hansotia T, Yusta B, Ris F, Halban PA, Drucker DJ. Glucagon-like peptide-1 receptor signaling modulates beta cell apoptosis. *J Biol Chem*. 2003; 278(1):471–478.
21. Garber AJ. Long-acting glucagon-like peptide 1 receptor agonists: a review of their efficacy and tolerability. *Diabetes Care*. 2011;34(suppl 2):S279–S284.
22. Kjems LL, Holst JJ, Volund A, Madsbad S. The influence of GLP-1 on glucose-stimulated insulin secretion: effects on beta-cell sensitivity in type 2 and nondiabetic subjects. *Diabetes*. 2003;52(2):380–386.
23. Hojberg PV, et al. Four weeks of near-normalisation of blood glucose improves the insulin response to glucagon-like peptide-1 and glucose-dependent insulinotropic polypeptide in patients with type 2 diabetes. *Diabetologia*. 2009;52(2):199–207.
24. Holst JJ, Knop FK, Vilsboll T, Krarup T, Madsbad S. Loss of incretin effect is a specific, important, and early characteristic of type 2 diabetes. *Diabetes Care*. 2011;34(suppl 2):S251–S257.
25. Knop FK, et al. Impaired incretin effect and fasting hyperglucagonaemia characterizing type 2 diabetic subjects are early signs of dysmetabolism in obesity. *Diabetes Obes Metab*. 2012;14(6):500–510.
26. Steiner DJ, Kim A, Miller K, Hara M. Pancreatic islet plasticity: interspecies comparison of islet architecture and composition. *Islets*. 2010;2(3):135–145.
27. Cabrera O, Berman DM, Kenyon NS, Ricordi C, Berggren PO, Caicedo A. The unique cytoarchitecture of human pancreatic islets has implications for islet cell function. *Proc Natl Acad Sci U S A*. 2006; 103(7):2334–2339.
28. Bosco D, et al. Unique arrangement of alpha- and beta-cells in human islets of Langerhans. *Diabetes*. 2010;59(5):1202–1210.
29. Rodriguez-Diaz R, et al. Alpha cells secrete acetylcholine as a non-neuronal paracrine signal priming beta cell function in humans. *Nat Med*. 2011; 17(7):888–892.
30. Rodriguez-Diaz R, et al. Innervation patterns of autonomic axons in the human endocrine pancreas. *Cell Metab*. 2011;14(1):45–54.
31. Hodson DJ, et al. Existence of long-lasting experience-dependent plasticity in endocrine cell networks. *Nat Commun*. 2012;3:605.
32. Schlegel W, et al. Oscillations of cytosolic Ca2+ in pituitary cells due to action potentials. *Nature*. 1987; 329(6141):719–721.
33. Rorsman P, Braun M, Zhang Q. Regulation of calcium in pancreatic alpha- and beta-cells in health and disease. *Cell Calcium*. 2012;51(3–4):300–308.
34. Quesada I, et al. Glucose induces opposite intracellular Ca2+ concentration oscillatory patterns in identified alpha- and beta-cells within intact human islets of Langerhans. *Diabetes*. 2006; 55(9):2463–2469.
35. Serre-Beinier V, et al. Cx36 makes channels coupling human pancreatic beta-cells, and correlates with insulin expression. *Hum Mol Genet*. 2009; 18(3):428–439.
36. Ravier MA, et al. Loss of connexin36 channels alters beta-cell coupling, islet synchronization of glucose-induced Ca2+ and insulin oscillations, and basal insulin release. *Diabetes*. 2005;54(6):1798–1807.
37. Head WS, Orseth ML, Nunemaker CS, Satin LS, Piston DW, Benninger RK. Connexin-36 gap junctions regulate in vivo first- and second-phase insulin secretion dynamics and glucose tolerance in the conscious mouse. *Diabetes*. 2012;61(7):1700–1707.
38. Zhang Q, et al. Cell coupling in mouse pancreatic beta-cells measured in intact islets of Langerhans. *Philos Trans A Math Phys Eng Sci*. 2008;366:3503–3523.
39. Li D, et al. Imaging dynamic insulin release using a fluorescent zinc indicator for monitoring induced exocytotic release (ZIMIR). *Proc Natl Acad Sci U S A*. 2011;108(52):21063–21068.
40. Maedler K, Oberholzer J, Bucher P, Spinas GA, Donath MY. Monounsaturated fatty acids prevent the deleterious effects of palmitate and high glucose on human pancreatic beta-cell turnover and function. *Diabetes*. 2003;52(3):726–733.
41. Poitout V. Beta-cell lipotoxicity: burning fat into heat? *Endocrinology*. 2004;145(8):3563–3565.
42. Muscelli E, et al. Separate impact of obesity and glucose tolerance on the incretin effect in normal subjects and type 2 diabetic patients. *Diabetes*. 2008; 57(5):1340–1348.
43. Joseph JW, et al. Free fatty acid-induced beta-cell defects are dependent on uncoupling protein 2 expression. *J Biol Chem*. 2004;279(49):51049–51056.
44. Allagnat F, Alonso F, Martin D, Abderrahmani A, Waeber G, Haefliger JA. ICER-1gamma overexpression drives palmitate-mediated connexin36 down-regulation in insulin-secreting cells. *J Biol Chem*. 2008;283(9):5226–5234.
45. Mears D, Sheppard NF, Atwater I, Rojas E. Magnitude and modulation of pancreatic beta-cell gap junction electrical conductance in situ. *J Membr Biol*. 1995;146(2):163–176.
46. Ravier MA, Sehlin J, Henquin JC. Disorganization of cytoplasmic Ca(2+) oscillations and pulsatile insulin secretion in islets from ob/ obmice. *Diabetologia*. 2002; 45(8):1154–1163.
47. Zhang M, et al. Long lasting synchronization of calcium oscillations by cholinergic stimulation in isolated pancreatic islets. *Biophys J*. 2008; 95(10):4676–4688.
48. Carvalho CP, et al. Impaired beta-cell-beta-cell coupling mediated by Cx36 gap junctions in prediabetic mice. *Am J Physiol Endocrinol Metab*. 2012; 303(1):E144–E151.
49. Winzell MS, Ahren B. The high-fat diet-fed mouse: a model for studying mechanisms and treatment of impaired glucose tolerance and type 2 diabetes. *Diabetes*. 2004;53(suppl 3):S215–S219.
50. Miller MR, et al. Levels of free fatty acids (FFA) are associated with insulin resistance but do not explain the relationship between adiposity and insulin resistance in Hispanic Americans: the IRAS Family Study. *J Clin Endocrinol Metab*. 2012; 97(9):3285–3291.
51. Knop FK, Aaboe K, Vilsboll T, Madsbad S, Krarup T, Holst JJ. Reduced incretin effect in obese subjects with normal glucose tolerance as compared to lean control subjects. *Diabetologia*. 2008;51:S258–S258.
52. Schafer SA, et al. Impaired glucagon-like peptide-1-induced insulin secretion in carriers of transcription factor 7-like 2 (TCF7L2) gene polymorphisms. *Diabetologia*. 2007;50(12):2443–2450.
53. Vilsboll T, Krarup T, Deacon CF, Madsbad S, Holst JJ. Reduced postprandial concentrations of intact biologically active glucagon-like peptide 1 in type 2 diabetic patients. *Diabetes*. 2001; 50(3):609–613.
54. Houslay MD, Milligan G. Tailoring cAMP-signalling responses through isoform multiplicity. *Trends Biochem Sci*. 1997;22(6):217–224.
55. Dulin NO, Niu J, Browning DD, Ye RD, Voyno-Yasenetskaya T. Cyclic AMP-independent activation of protein kinase A by vasoactive peptides. *J Biol Chem*. 2001;276(24):20827–20830.
56. Ma Y, Pitson S, Hercus T, Murphy J, Lopez A, Woodcock J. Sphingosine activates protein kinase A type II by a novel cAMP-independent mechanism. *J Biol Chem*. 2005;280(28):26011–26017.
57. Hu W, Bielawski J, Samad F, Merrill AH, Cowart LA. Palmitate increases sphingosine-1-phosphate in C2C12 myotubes via upregulation of sphingosine kinase message and activity. *J Lipid Res*. 2009; 50(9):1852–1862.
58. Tian G, Sandler S, Gylfe E, Tengholm A. Glucose- and hormone-induced cAMP oscillations in alpha- and beta-cells within intact pancreatic islets. *Diabetes*. 2011;60(5):1535–1543.
59. Hoppa MB, et al. Chronic palmitate exposure inhibits insulin secretion by dissociation of Ca(2+) channels from secretory granules. *Cell Metab*. 2009; 10:455–465.
60. Collins SC, et al. Progression of diet-induced diabetes in C57BL6J mice involves functional dissociation of Ca2(+) channels from secretory vesicles. *Diabetes*. 2010;59(5):1192–1201.
61. Gehrmann W, Elsner M, Lenzen S. Role of metabolically generated reactive oxygen species for lipotoxicity in pancreatic beta-cells. *Diabetes Obes Metab*. 2010;12(suppl 2):149–158.
62. Benninger RK, Zhang M, Head WS, Satin LS, Piston DW. Gap junction coupling and calcium waves in the pancreatic islet. *Biophys J*. 2008;95(11):5048–5061.
63. Stozer A, et al. Functional connectivity in islets

of Langerhans from mouse pancreas tissue slices. *PLoS Comput Biol*. 2013;9(2):e1002923.
64. Stozer A, Dolensek J, Rupnik MS. Glucose-stimulated calcium dynamics in islets of Langerhans in acute mouse pancreas tissue slices. *PLoS One*. 2013; 8(1):e54638.
65. Ellacott KL, Morton GJ, Woods SC, Tso P, Schwartz MW. Assessment of feeding behavior in laboratory mice. *Cell Metab*. 2010;12(1):10–17.
66. Hodson DJ, et al. Coordination of calcium signals by pituitary endocrine cells in situ. *Cell Calcium*. 2012; 51(3–4):222–230.
67. Kang ZF, et al. Pharmacological reduction of NEFA restores the efficacy of incretin-based therapies through GLP-1 receptor signalling in the beta cell in mouse models of diabetes. *Diabetologia*. 2013; 56(2):423–433.
68. Marchetti P, et al. A local glucagon-like peptide 1 (GLP-1) system in human pancreatic islets. *Diabetologia*. 2012;55(12):3262–3272.
69. Panjwani N, et al. GLP-1 receptor activation indirectly reduces hepatic lipid accumulation but does not attenuate development of atherosclerosis in diabetic male ApoE($^{-/-}$) mice. *Endocrinology*. 2013; 154(1):127–139.
70. Rocheleau JV, et al. Critical role of gap junction coupled KATP channel activity for regulated insulin secretion. *PLoS Biology*. 2006;4(2):e26.
71. Ravier MA, Rutter GA. Glucose or insulin, but not zinc ions, inhibit glucagon secretion from mouse pancreatic alpha-cells. *Diabetes*. 2005; 54(6):1789–1797.
72. Sanchez-Cardenas C, et al. Pituitary growth hormone network responses are sexually dimorphic and regulated by gonadal steroids in adulthood. *Proc Natl Acad Sci U S A*. 2010;107(50):21878–21883.